An Electron Microscopic and Optical Diffraction Analysis of the Structure of *Limulus* Telson Muscle Thick Filaments

ROBERT W. KENSLER and RHEA J. C. LEVINE
Department of Anatomy, The Medical College of Pennsylvania, Philadelphia, Pennsylvania 19129

ABSTRACT Long, thick filaments (>4.0 μm) rapidly and gently isolated from fresh, unstimulated *Limulus* muscle by an improved procedure have been examined by electron microscopy and optical diffraction. Images of negatively stained filaments appear highly periodic with a well-preserved myosin cross-bridge array. Optical diffraction patterns of the electron micrographs show a wealth of detail and are consistent with a myosin helical repeat of 43.8 nm, similar to that observed by x-ray diffraction. Analysis of the optical diffraction patterns, in conjunction with the appearance in electron micrographs of the filaments, supports a model for the filament in which the myosin cross-bridges are arranged on a four-stranded helix, with 12 cross-bridges per turn of each helix, thus giving an axial repeat every third level of cross-bridges (43.8 nm).

Abundant evidence exists that contraction in striated muscle fibers occurs by a sliding filament mechanism in which thin filaments containing actin interact with thick filaments containing myosin to produce tension (14, 16). Although x-ray diffraction analysis of muscle has been extremely successful in defining the helical repeat of the myosin cross-bridges of the thick filament in a variety of vertebrate and invertebrate striated muscles (9, 11, 12, 15, 19, 20, 27, 32, 33, 36), a number of major questions still remain unanswered about the structure of thick filaments. In particular, the number of helical strands (or the number of myosins at each 14.6-nm level) is not known for any filament. In vertebrate muscle, biochemical estimates suggest that there are either three or four myosins every 14.3 nm (21, 24, 31), arranged on either a two-, three-, or four-stranded helical lattice (12, 15, 22, 23, 28, 29), while in insect flight muscle it is not yet clear whether the myosin filament structure is four- or six-stranded (2, 25, 30, 31, 34). The number of myosin heads at each level along the filament is likewise unknown for the thick filaments in striated muscle from *Limulus* (35, 36), scallop (36), and lobster and crayfish (32, 33, 36). The question of the number of cross-bridges present at each level in these filaments is of great importance not only in terms of understanding how the myosin is arranged in the thick filament but also in understanding how the filament interacts with adjacent actin filaments.

In this paper we discuss the structure of *Limulus* thick filaments isolated in their long conformation as revealed by electron microscopy and optical diffraction analysis of the micrographs. Based on these studies, evidence is presented for the presence of four myosin cross-bridges at each 14.6-nm level of the filament.

MATERIALS AND METHODS

Filament Isolation

Thick filaments were isolated from the median telson levator muscles of *Limulus polyphemus* by a modification of the technique of Hardwicke and Hanson (10). Small bundles of unstimulated muscle, quickly dissected from the animal with the tendon insertions intact, were immersed for ~10 min in a mincing solution containing 0.1 M NaCl, 2 mM EGTA, 1 mM dithiothreitol (DTT), 5 mM $MgCl_2$, and 7 mM phosphate buffer (pH 7.2) at 4°C. This temperature was maintained throughout the subsequent steps of the isolation procedure. The muscle was then cut at one end, gently teased into fine bundles (0.5 mm diameter), and immersed in freshly made mincing solution in which the 0.1 M NaCl was replaced with 0.1 M KCl. We have found that this procedure minimized contraction of the freed bundles. Reference to the small contractions observed when bundles were initially immersed in a solution containing 0.1 M KCl can be found in Dewey et al. (7). After 4 h in this solution, the bundle was finely minced with a razor blade and homogenized in relaxing solution containing 0.1 M KCl, 5 mM $MgCl_2$, 1 mM EGTA, 1 mM DTT, 2.5 mM ATP in 7 mM phosphate buffer (pH 7). (In some cases, preparations were left in mincing solution overnight, with no deleterious effects. 4 h was chosen for convenience, although filaments could be successfully isolated, at a lower yield, after soaking times as short as 2 h.) The muscle mince was homogenized, on ice, in two 15-s bursts (separated by 30 s) at setting 3 of the Sorvall Omnimixer (DuPont Co., Wilmington, Del.) using the 5 ml mini-cup. The homogenate was diluted with relaxing solution to ~15 ml and centrifuged at 3,000 *g* for 10 min at 4°C. The separated filaments in the supernatant were collected for examination.

Electron Microscopy

For negative staining, isolated filaments were adsorbed to grids coated with a thin carbon film (50–75 Å) supported by a perforated Formvar film. After ~30 s, the grids were rinsed with 0.1 M ammonium acetate (10) and negatively stained with 1% uranyl acetate.

Electron microscopy of negatively stained isolated thick filaments was performed on a Philips EM 300 electron microscope at 80 kV. The magnification of each cassette of plates was calibrated by photographing a grid of negatively

© The Rockefeller University Press · 0021-9525/82/02/0443/09 $1.00

stained catalase crystals (37) at the same magnification. To further reduce variations in magnification, each cassette of plates was photographed without varying the magnification between exposures.

Thick filaments, lying on the carbon over the holes in the Formvar film, were photographed at nominal magnifications of × 10,000 and 20,000 for optical diffraction analysis and measurements of filament length. Measurements of the diameter of the filaments at the bare zone and in the region of the myosin cross-bridges were made on micrographs at × 50,000–80,000, using an optical micrometer.

Optical Diffraction Analysis

Electron micrograph negatives of isolated thick filaments taken at initial magnifications of × 10,000 or 20,000 were diffracted in a laser optical diffractometer (1) according to standard procedures (4, 13, 17). The diffractometer used the coherent light from a 2 mW helium-neon laser (632.8 nm) and had a specimen-to-film length of 3.5 meters. Most of the diffraction patterns were obtained directly from the original micrographs rather than from photographic copies, and were recorded on Polaroid type 55 film. The diffractometer camera constant was computed from diffraction patterns of micrographs of catalase crystals (8.7-nm spacing). Measurements of the diffraction pattern spacings were made on enlarged copies of the transforms (14.6 nm^{-1} = ~20 nm) with a vernier caliper device accurate to 0.05 mm.

Modeling of Filament Appearance

Models of the anticipated appearance of filaments with four cross-bridges at each 14.6-nm level and an axial repeat of 43.8 nm were constructed using a computer program which allowed the projected appearance of a model filament in two dimensions to be calculated. The cross-bridges were modeled as cylinders with rounded ends 5.6 × 15.0 nm (36), centered at a radius of r = 16.0 nm. The axial tilt and azimuthal tilt angles of the cross-bridges were defined as illustrated by Wray et al. (36) and Haselgrove (12). The positions of the cross-bridges were calculated relative to an x, y, z coordinate system in which the z axis was selected to represent the filament axis. For purposes of computation, using a Texas Instruments 59 programmable calculator, the two ends of the cross-bridge were represented by two spheres 5.6 nm in diameter separated by 9.4 nm. By setting the center of mass of the first cross-bridge at x, y, z coordinates of $0, r, 0$ and given the selected axial tilt and aximuthal tilt angles for the cross-bridge, the program first calculated the x, y, z coordinates of the centers of the two spheres representing the ends of the first cross-bridge. Given these coordinates for the first cross-bridge, the angular rotation between adjacent cross-bridges (both at the same level and at adjacent 14.6-nm levels), and a axial rise of z = 14.6 nm between cross-bridge levels, the program calculated the corresponding Cartesian coordinates for the midpoints of the ends of each cross-bridge in the helical array. To construct the model, the x, z coordinates of the midpoints of the ends of each cross-bridge were plotted on graph paper on an x, z coordinate system, and circles scaled to represent 5.6-nm diameter were constructed around each of these points to define the ends of the cross-bridges. The circles corresponding to the two ends of the same cross-bridge were connected by straight lines. The image constructed by hand on graph paper corresponds to the appearance of the model filament profile as projected on the x, z plane. The appearance of the model as it would appear rotated about its axis was constructed by computing the Cartesian coordinates for the first bridge rotated by the selected number of degrees from its first position, and then by calculating the positions of all the other cross-bridges relative to the new position of this cross-bridge.

RESULTS

Electron Microscopic Appearance of the Filaments

A prime requirement for the analysis of thick filament structure from electron micrographs is optimal preservation of native filament structure. Our initial studies of negatively stained *Limulus* thick filaments indicated that the myosin cross-bridges of filaments rapidly isolated from fresh muscle were much better preserved than those of filaments isolated from glycerinated muscle. The present procedure, a modification of the technique of Hardwicke and Hanson (10), consistently yields populations (Fig. 1) of *Limulus* thick filaments of uniform length (4.1 ± 0.2 μm SD, n = 100) with well-ordered arrays of myosin cross-bridges. The filaments possessed distinct central bare zones and, even in low magnification electron micrographs (Fig. 1), appeared highly periodic along their length. At higher magnification (Figs. 2, 3 *a–c*, and 4), the myosin cross-bridge periodicity along the filaments was even more striking and can be seen particularly well by tilting the photographs and sighting along the length of individual filaments. The projection of the cross-bridges away from the filament surface is apparent at many points (Figs. 3 *a–c* and 4, arrows). Where a thick filament lies adjacent to a thin filament, the contact between myosin cross-bridges and the actin of the thin filament can be seen at regular intervals (Fig. 3 *a*). Careful inspection of high magnification electron micrographs revealed that the cross-bridges appeared to be paired, so that cross-bridges projected from opposite sides of the filament at the same level. Maximum filament diameter, measured at these points, averaged 36.3 ± 1.6 nm SD (n = 238). Taking the filament diameter in the region of the bare zone, measured as 23.4 ± 1.3 nm SD (n = 36), as representative of shaft diameter, we calculated that the myosin cross-bridges projected 6.5 nm from the filament surface.

The myosin cross-bridge pattern repeated every third level of cross-bridges (Figs. 3 *a–c* and 4). Measurements of this periodicity, made from enlarged prints (× 365,000; 1 mm = 2.7 nm) of the thick filaments, averaged 42.8 ± 1.5 nm SD (n = 33). For this calculation, a length of 18–20 repeats was measured along each filament and divided by the actual number of repeats to give the mean periodicity for that filament. 33 filaments were measured in this way, and the mean of the values was calculated.

Optical Diffraction

The electron micrographs of the *Limulus* thick filaments consistently gave strong optical diffraction patterns (Figs. 3 *d–f*) with meridional reflections at 14.6 and 7.3 nm^{-1} and, occasionally, at 4.9 nm^{-1} as well. Off-meridional reflections occurred on layer lines which indexed close to the first, second, fourth, and fifth orders of a 43.8 nm^{-1} helical repeat (Table I). The first, third, and fourth layer lines were relatively strong, while the second and fifth were weak. Moderately strong subsidiary reflections were associated with the 14.6 nm^{-1} meridional reflection. In diffraction patterns of filaments masked so that the mask transform spikes would not coincide with the equatorial plane of the filament transform, equatorial reflections at ~7.0 nm^{-1} were also present. Qualitatively, this diffraction pattern was very similar (Fig. 6) to the x-ray diffraction pattern obtained by Wray et al. (35) from relaxed *Limulus* muscle. This indicated that the native order of the myosin cross-bridges of the filaments was preserved during negative staining and, further, implied that the appearance of the filaments in the electron micrographs reflected their *in situ* structure reasonably well.

The major diffraction maxima of the optical diffraction pattern were indexed on reciprocal nets (Fig. 7) corresponding to the near and far surfaces of the helix. The reciprocal nets corresponded to an n, L plot of an equation of the form $L = n/N + 3m$, where L is the layer line number, n is the order of the Bessel function predicted for that layer line, N is the rotational symmetry, and m is an integer (see reference 3).

Calculations (Table I) of the radius at which the cross-bridges are centered and an estimate of the rotational symmetry (N) of the *Limulus* filament were made from the radial positions (relative to the meridian) of the subsidiary maxima on the 14.6 nm^{-1} meridional layer line and the primary maxima on the first layer line. Using filament models, Wray et al. (36) and

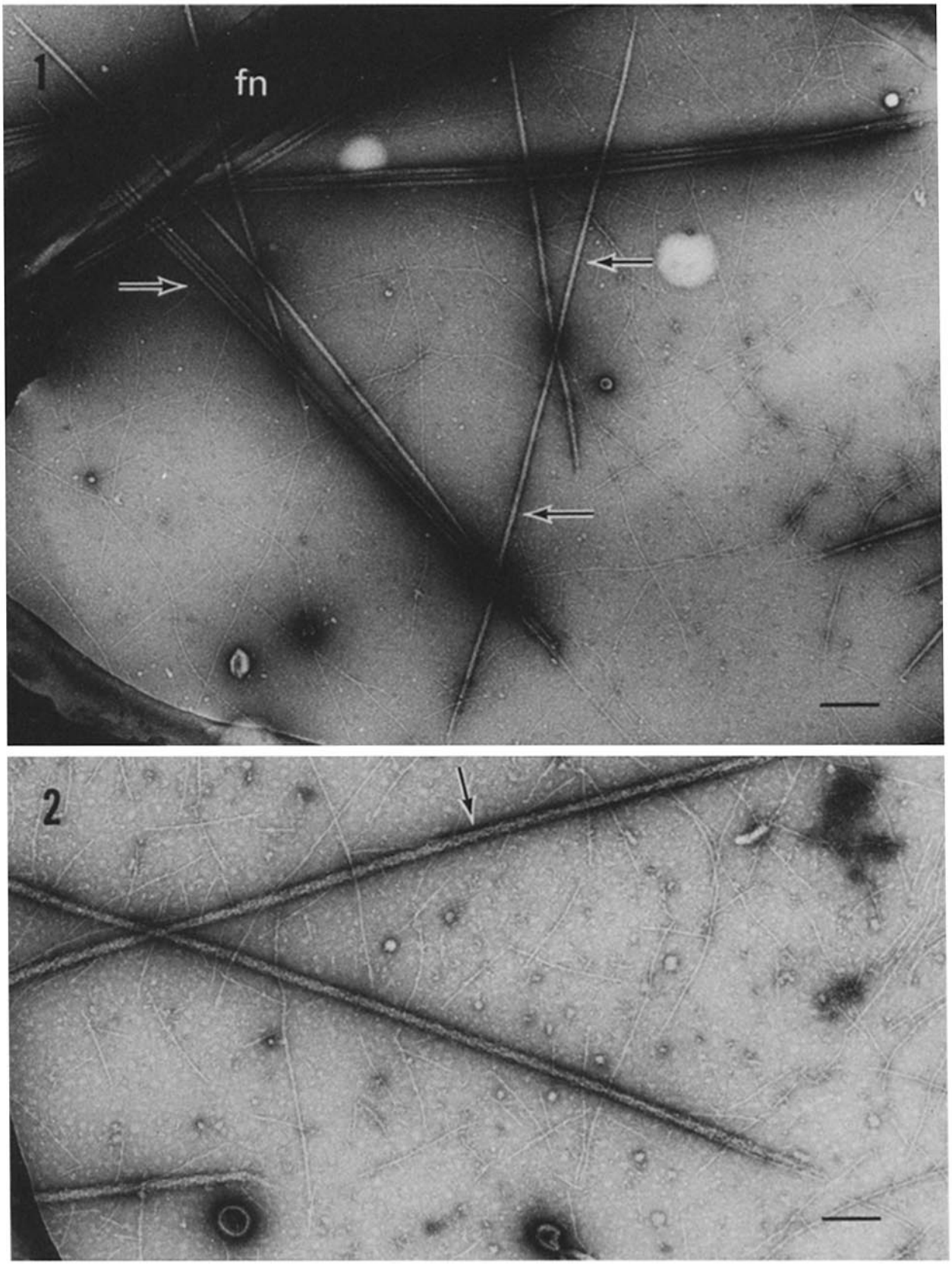

FIGURE 1 A low-magnification electron micrograph of negatively stained *Limulus* thick filaments illustrating the long length and uniformity of the filaments. Regions of periodicity along the filaments can be seen at the arrows. *fn*, Formvar net. Bar, 0.35 μm. × 28,600.

FIGURE 2 A medium-magnification electron micrograph illustrating the periodicity of the myosin cross-bridges along the filaments. Actin thin filaments can be seen in the background and in association with one of thick filaments at the arrow. Bar, 0.15 μm. × 67,900.

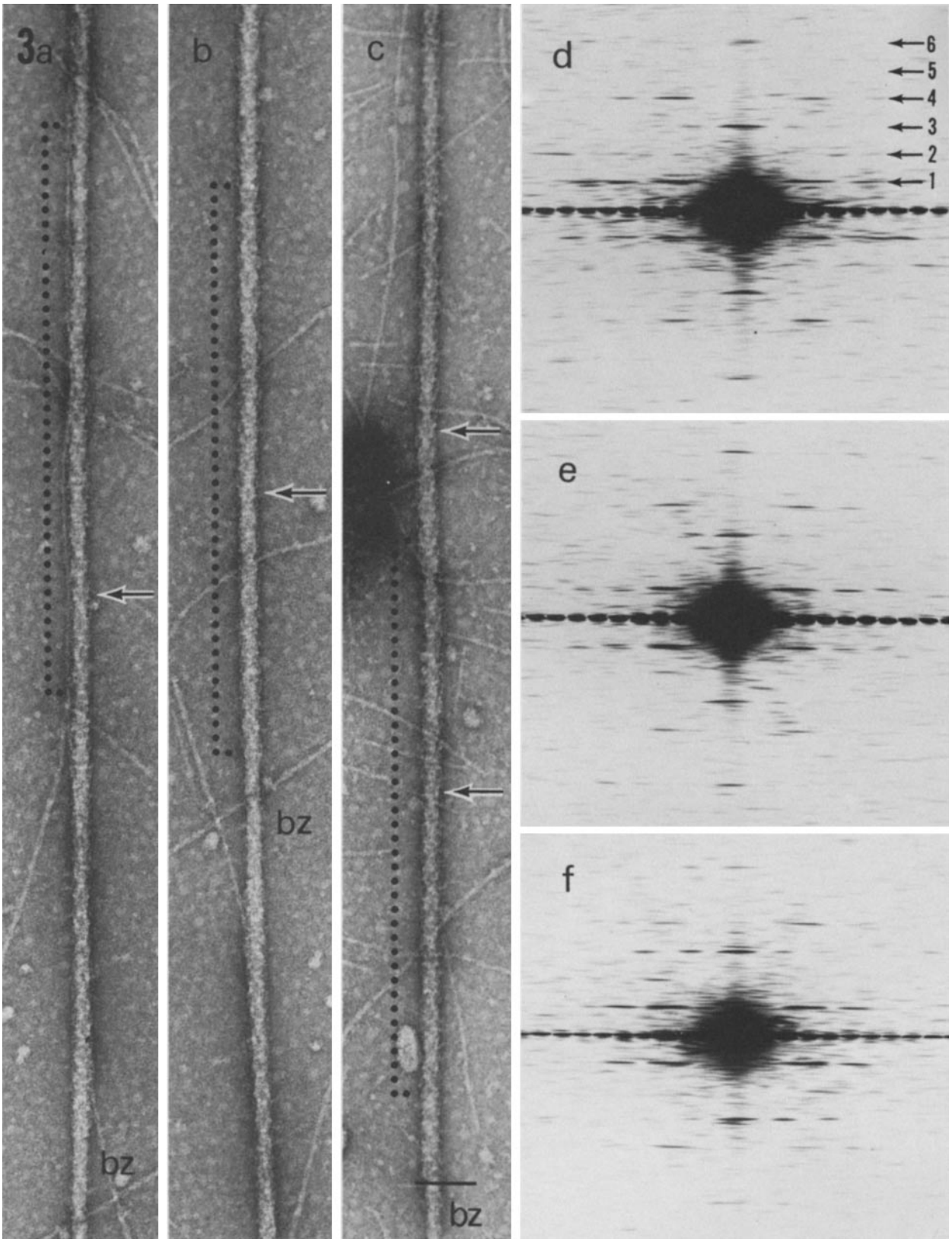

FIGURE 3 Medium-magnification electron micrographs of three regions of thick filaments (*a–c*) and their corresponding optical diffraction patterns (*d–f*). The patterns were taken from the region of the filaments indicated by the rows of dots. Regions *a* and *b* are of the opposite ends of the same filament and illustrate the long length of the filaments. The bare zone (*bz*) is indicated. Note the highly periodic structure of the filaments and the hexagonal surface pattern, repeating at 43.8-nm intervals (arrows). The optical diffraction patterns (*d–f*) illustrate the consistently detailed nature of the patterns with layer lines at (*1*) 43.8, (*2*) 21.9, (*3*) 14.6, (*4*) 10.9, and (*5*) 7.3 nm^{-1}, and the subsidiary maxima on the (*6*) 14.6 nm^{-1} layer line. Bar, 0.1 μm. × 111,500.

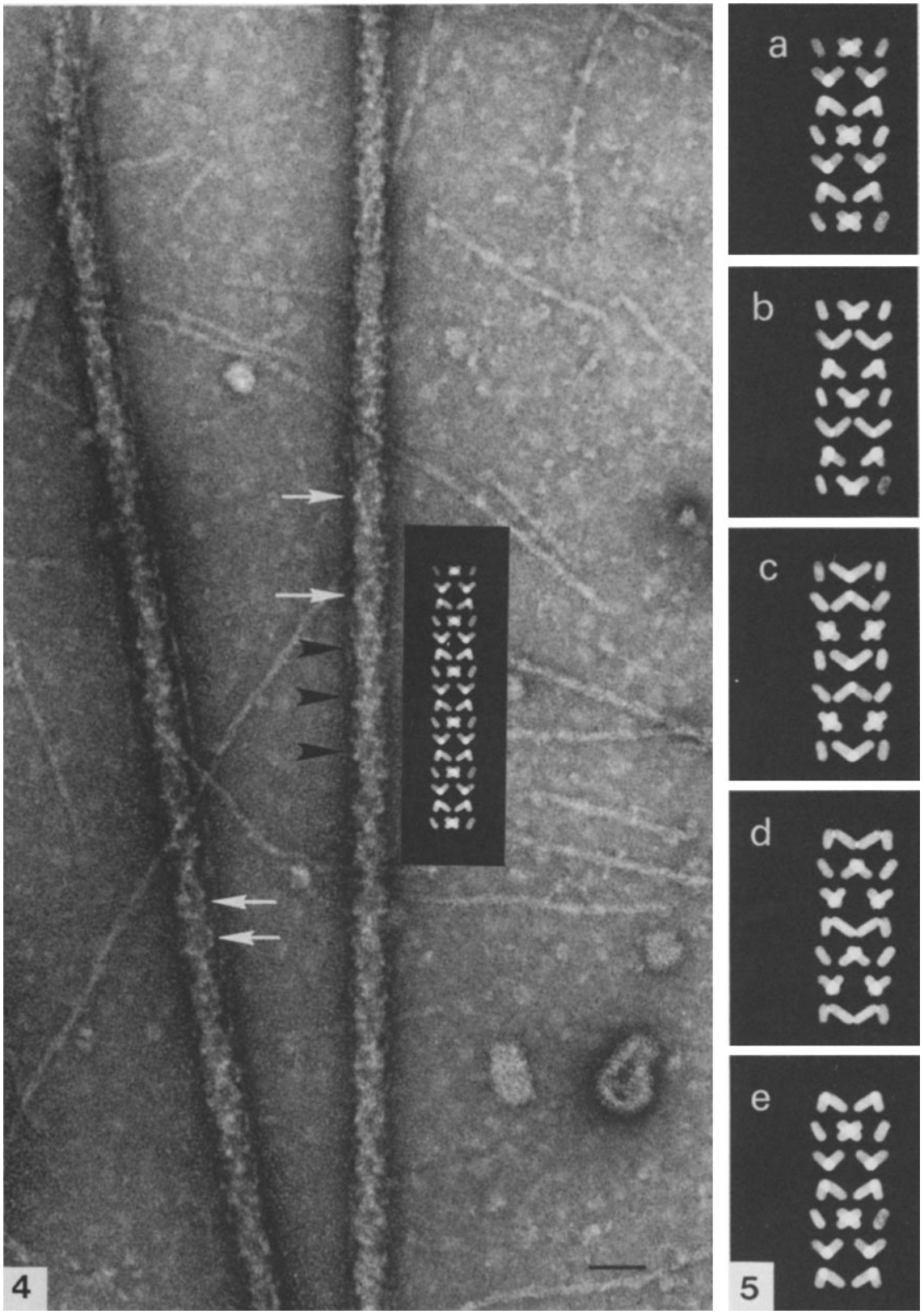

FIGURE 4 A comparison of one of the views of the model together with a high-power electron micrograph of the filaments illustrating their similarity in appearance. Note that the model provides an explanation for the pairs of white dots (white arrows) and hexagonal pattern (arrowheads) seen at many points along the filament. Bar, 50 nm. × 204,000.

FIGURE 5 Illustrations of the expected myosin cross-bridge patterns for a filament with four myosin cross-bridges at each 14.6-nm level arranged in a 12/4 helix. The positions of the cross-bridges were calculated for the drawings as described in Materials and Methods, using axial and azimuthal tilt angles of 35° and 70° for the cross-bridges. The different images (*a–e*) represent the expected appearances of a region of the model filament as it is rotated around its longitudinal axis from 0° (*a*) to 30° (*e*) in 7.5° increments. Note that the pattern in *e* is the same as in *a* but shifted one level of bridges down. The model images also illustrate schematically that white (low density, stain excluding) regions may occur at the points where the cross-bridges on the near and far sides of the filament appear to overlap in the projected view.

TABLE I

Diffraction Pattern Measurements

A. Layer line (LL) spacing

LL	Mean ± SD	n*	% Deviation of mean values from L/43.8
	nm		
1	43.2 ± 1.3	49	1.4
2	22.1 ± 0.4	49	0.9
3	14.6 ± 0.1	49	0
4	10.9 ± 0.1	49	0.45
5	8.8 ± 0.1	15	0.46
6	7.3 ± 0.1	19	0
7	—	—	—
8	—	—	—
9	4.8 ± 0.1	7	1.25

B. Radial spacings from meridian of diffraction maxima‡

	nm^{-1} ± *SD*
Primary maxima on 1st LL (43.2 nm^{-1})	17.8 ± 1.8 (n = 49)
Secondary maxima on 1st LL (43.2 nm^{-1})	10.3 ± 0.7 (n = 47)
Primary maxima on 4th LL (10.9 nm^{-1})	18.2 ± 2.1 (n = 49)
Secondary maxima on 4th LL (10.9 nm^{-1})	10.2 ± 0.9 (n = 17)
First subsidiary maxima on 3rd LL (14.6 nm^{-1})	25.7 ± 2.6 (n = 39)
Secondary subsidiary maxima on 3rd LL (14.6 nm^{-1})	13.8 ± 0.8 (n = 9)

C. Calculated cross-bridge radius

	nm
Based on radial spacing (25.7 nm^{-1}) of 1st 14.6 nm^{-1} subsidiary maxima	15.5
Based on radial spacing (13.8 nm^{-1}) of 2nd 14.6 nm^{-1} subsidiary maxima	15.3

D. Comparison of calculated maxima ($2\pi rR$) for Bessel function describing position of primary maxima on 1st LL and table values

Measurements Used	$2\pi rR$ Calculated	Table values, J_n
Using calculated radius of bridges (15.5 nm) and calculated radial spacing of primary maxima on 1st LL (17.8 nm^{-1})	5.5	4.2 (J_3), 5.32 (J_4), 6.4 (J_5)

* Number of diffraction patterns measured.

‡ The 2nd and 5th LL were frequently too weak for accurate measurement of the positions of the diffraction maxima.

Haselgrove (12) have shown that the positions of the subsidiary maxima on the meridional layer line are primarily dependent on the radius at which the cross-bridges are centered. Since the profile of these maxima is specified by a zero-order Bessel function, it is possible to calculate the radius (r) at which the cross-bridges are centered. The position of the secondary maximum of the zero-order Bessel function, J_0, is given by $2\pi rR = 3.8$, where R is the radical spacing, measured from the meridian, of the subsidiary maxima. The radial spacing of the subsidiary maxima (Table I), measured from the optical diffraction patterns, was 25.7 ± 2.6 nm^{-1} SD (n = 77), and the cross-bridges were calculated to be centered at a radius of 15.5 nm. The radial position of the main peak on the first layer line is governed both by the radial position of the cross-bridges and by the number of strands on the myosin helix: the rotational symmetry, N (12, 30, 36). Using the calculated center of radius of the cross-bridges (r = 15.5 nm) and the measured radial position of the primary maxima on the first layer line (R = 17.8 nm^{-1}), we calculated a value ($2\pi rR$) of 5.5 for the Bessel function describing the position of the primary maxima on the first layer line. This is closest to the expected maximum (5.32) of a J_4 Bessel function, corresponding to a rotational symmetry of 4 (Table I *D*). From the diffraction patterns alone, however, neither we nor Wray et al. (35, 36) could entirely rule out rotational symmetries of 3 or 5 for the filaments. Close inspection of our high power electron micrographs (Fig. 4), however, revealed that the filaments showed mirror plane symmetry across the central longitudinal axis, in many regions. Thus, the filaments appear bilaterally symmetric, in projection along their long axes. Symmetry of this type would be most likely to occur if the filament has an even rotational symmetry, such as 4, not 3 or 5.

Our results, therefore, support the interpretation of a myosin cross-bridge arrangement in which there are four helical chains of cross-bridges, each consisting of 12 cross-bridges per turn. The filaments would thus display four cross-bridges at each 14.6-nm level and an axial repeat at every third level of cross-bridges.

Models of the Filament

On the basis of the above interpretation regarding the arrangement of myosin cross-bridges, we have modeled the expected appearance of such a filament, projected onto a plane corresponding to an electron microscopic image. In our computations, the myosin cross-bridge was modeled as a cylinder with rounded ends 5.6 × 15.0 nm (36) centered at a radius of 16 nm. The axial and azimuthal tilt angles of the cross-bridges were defined as described by Wray et al. (36) and Haselgrove (12); and models with cross-bridges at various axial tilt and azimuthal angles were computed. Although variations in the tilt angles do produce slight changes in appearance of the models, the structures shown in Figs. 5 *a–e* are typical of the computed images and illustrate the major appearances expected for the filament, when rotated around its longitudinal axis from 0° to 30°. As one continues to rotate the model, images similar to Fig. 5 *a–e* recur. We note a good resemblance between these computed models and images of the real filaments (Fig. 4). The model accounts for the prominent stain-excluding (white) regions which appear to occur centrally every third level of bridges along the filament axis and the frequently seen pairs of white dots (Fig. 4, white arrows) which occur at successive levels of the filament. As illustrated in the model, these dots may represent the regions at which the cross-bridges at the back and front of the helix appear to overlap in the projected view. Although the model and the real filament do differ in some aspects, this is to be expected since the model presents only the profiles of the bridges and not differences in density due to factors such as the tilt angle of the bridge or its shape. Optical diffraction patterns of photographs of the models also simulate many features of the diffraction patterns of the native filaments. While these studies do not absolutely prove the validity of the model, they do suggest that the

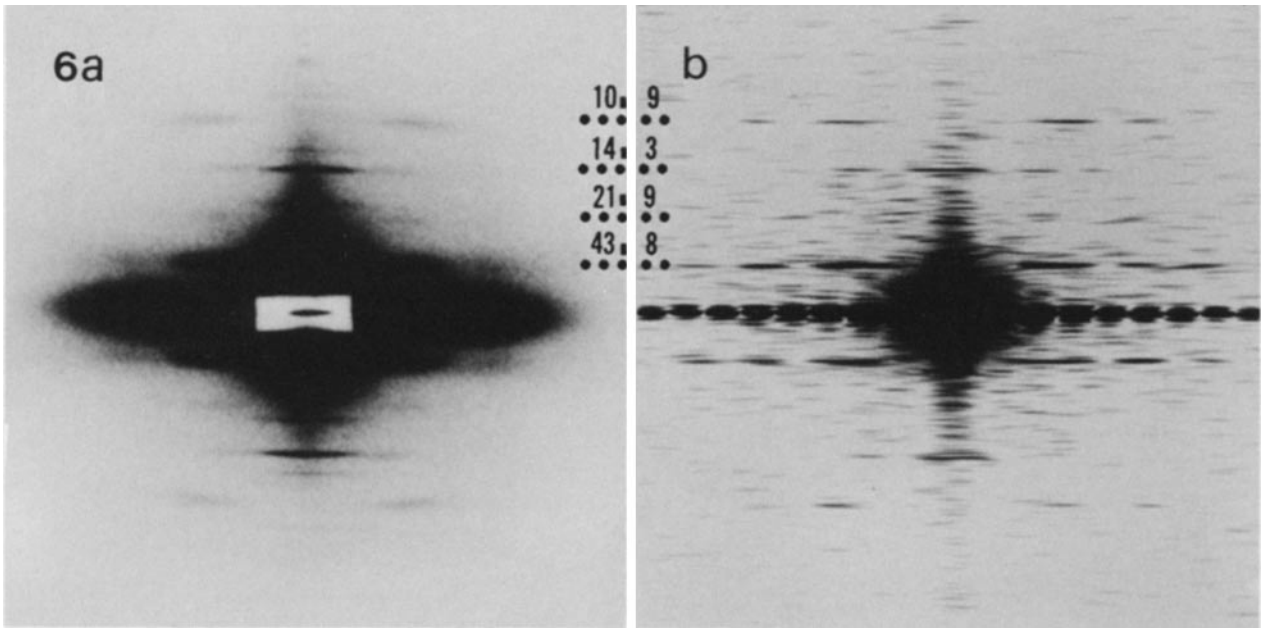

FIGURE 6 A comparison of an x-ray diffraction pattern obtained from unstimulated *Limulus* muscle (*a*) and an optical diffraction pattern obtained from an isolated *Limulus* thick filament (*b*). Note that the patterns are similar in that the layer lines occur as orders of an ~43.8 nm^{-1} repeat, with the first and fourth layer lines being strong, while the second layer line is relatively weak. The presence of subsidiary maxima associated with the 14.6-nm^{-1} meridional layer line is also evident in both patterns. *a* is reprinted with permission from Wray, J., P. Vibert, and C. Cohen, 1974, *J. Mol. Biol.* 88:343–348.

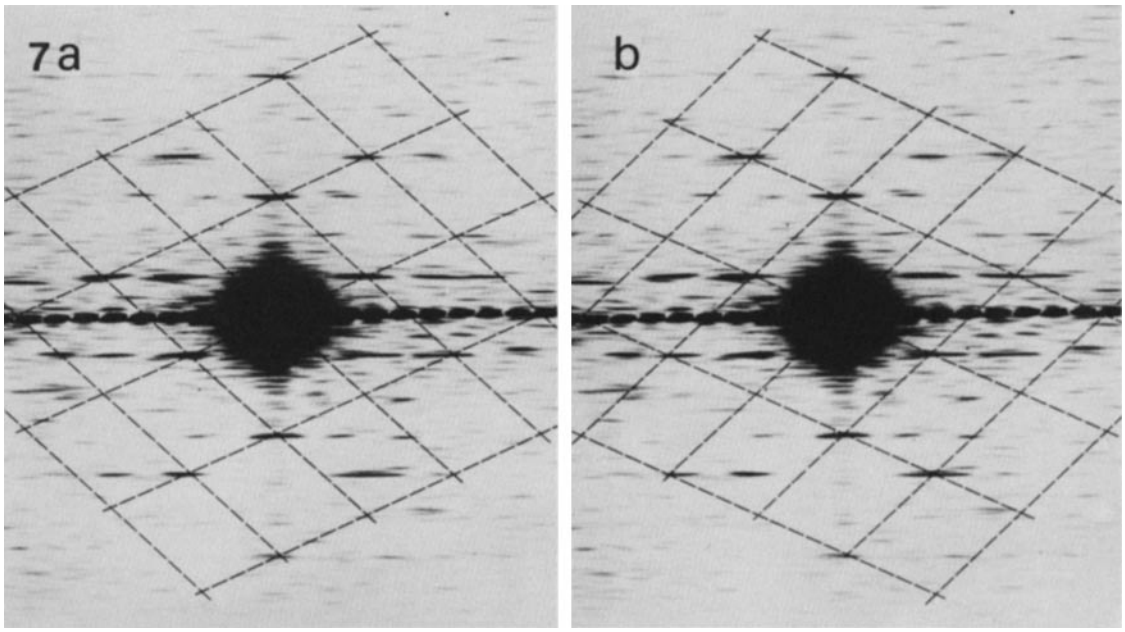

FIGURE 7 An optical diffraction pattern indicating the tentative indexing of the major diffraction maxima on reciprocal nets corresponding to the far (*a*) and near (*b*) sides of filament. Note the relative similarity of the corresponding diffraction maxima from the near and far sides of the filament both in their radial distances from the meridian and in their intensities. This similarity indicates good preservation and staining of both sides of the filament.

electron microscopic appearance of the *Limulus* thick filaments is consistent with the presence of four myosin cross-bridges at each 14.6-nm level arranged in a 12/4 helix.

DISCUSSION

As mentioned above, it is obvious that success in the analysis of thick filament structure from electron micrographs ultimately depends upon the optimal preservation of native filament structure. The results presented here demonstrate that *Limulus* thick filaments can be isolated with their myosin cross-bridges arranged in a highly ordered helical array, as shown by the strong and extremely detailed optical diffraction patterns we consistently obtain from electron micrographs of the filaments. The striking similarity between our optical diffraction

patterns and the x-ray diffraction patterns of relaxed *Limulus* muscle reported by Wray et al. (35, 36) provides further evidence that the structure we observe corresponds to the *in situ* arrangement of the myosin cross-bridges on the relaxed thick filament.

Both our optical diffraction patterns and the x-ray diffraction patterns of *Limulus* muscle of Wray et al. (35, 36) reveal a series of layer lines indexing close to the expected orders of a 43.8-nm helical repeat. Wray et al (35) interpreted these layer lines as arising from the helical array of myosin cross-bridges. Our electron micrographs support this interpretation and show a clear myosin helical repeat pattern of ~43.8 nm along the filament. The value of 15.5 nm, calculated from the optical diffraction patterns as the radius at which the cross-bridges are centered: (*a*) falls midway between the radius of the backbone (11.75 nm) and the farthest mean radius to which the cross-bridges appear to extend (18.5 nm), as measured on our electron micrographs; (*b*) is consistent with the value of ~16.5 (Wray et al. [35, 36]) for these filaments from x-ray diffraction; and (*c*) is also similar to the calculated radius at which the cross-bridges are centered in thick filaments of both lobster fast and scallop striated muscles (36).

Squire (28, 29) has proposed a general model for thick filament structure which predicts a rotational symmetry of 4 or 5 for filaments with the diameter of the *Limulus* thick filament. From their x-ray diffraction patterns, Wray et al. (35, 36) have proposed a rotational symmetry of 4 for the *Limulus* filament. They could not, however, rule out a rotational symmetry of 3 as a possibility. Our calculations of the spacings in the optical diffraction patterns, together with the appearance and dimensions of the filaments in electron micrographs, strongly support a rotational symmetry of 4 for the *Limulus* thick filament. Although n-stranded discontinuous helices of odd n can appear bilaterally symmetrical, this occurs only in special cases, such as when there is a rotation of $360°/(2 \times n)$ around the filament for each axial repeat, and then only in certain projected views. A consistently bilateral appearance would therefore occur only if the filaments always lie on the grid with the same orientation about their axes, which seems unlikely. The consistently bilateral appearance of the helical cross-bridge pattern of *Limulus* filaments argues against their showing even the special case of an odd n. Further support of our interpretation comes from models of filaments with 4 helical strands and 12 cross-bridges per helical turn, which are consistent in appearance with the images in electron micrographs of the *Limulus* filaments. The *Limulus* thick filament is thus the first filament for which the number of helical myosin strands is known with any degree of confidence. Results of computer image analysis of these filaments will be presented elsewhere.

There appears to be little relationship between the orderliness of thick filament structure and that of the overall array of thick filament within muscle fibers, however. Although individual thick filaments of *Limulus* telson levator muscles are highly periodic, they are disposed in a very irregular hexagonal lattice within the muscle fibers (8). Disorder is also apparent within the lattice, of from nine to twelve thin filaments (8). In contrast, the thick filament lattice of insect flight muscles is extremely regular—indeed, almost crystalline in appearance—and each thick filament is likewise surrounded by six, precisely positioned, thin filaments (25). Individual thick filaments of insect flight muscle, however, have a surface structure which appears far less well-ordered than does that of *Limulus* filaments (26). This may be related to the distance between the filament shaft and the cross-bridge mass, which appears to be greater for the insect than the *Limulus* filament. Other factors, however, may also influence fiber architecture. In insect flight muscle the regularity of the filament lattice appears to originate with the thin filaments and be imposed upon the thick filaments through their association with the thin. That this is clearly not the case in *Limulus* may relate to differences in functional requirements between the slow, primarily isotonic, telson muscle fibers, operating over great length ranges and the rapid, practically isometrically contracting, insect flight muscle fibers.

Knowledge of the structure of the *Limulus* thick filament is of considerable interest since extensive evidence exists that these filaments may shorten during isotonic contraction of the sarcomere below a rest length of ~7.0 μm (5–7, 18). The filaments studied here were all 4.0 μm or longer. Our analysis, thus, represents the structure of the filament in its long conformation. Similar studies are under way to determine the structure of the filament in its shortened conformation (~3.0 μm length), the structure of the paramyosin cores in both long and short filaments, and the hand of the myosin helix. The result of these studies will help to clarify the nature of the changes in the packing of myosin and paramyosin which occur during filament shortening.

We wish to thank Drs. M. Stewart and J. Haselgrove for helpful discussion, and Ms. Vanessa Rivers for secretarial assistance.

This work was supported by U. S. Public Health Service grants HL15835 (to the Pennsylvania Muscle Institute) and GM07475.

Received for publication 15 June 1981, and in revised form 21 September 1981.

REFERENCES

1. Berger, J. E., C. R. Zobel, and P. E. Engler. 1966. Laser as light source for optical diffractometers: Fourier analysis of electron micrographs. *Science (Wash. D. C.).* 153:168–169.
2. Chaplain, R. A., and R. T. Tregear. 1966. The mass of myosin per cross-bridge in insect fibrillar flight muscle. *J. Mol. Biol.* 21:275–280.
3. Cochran, W., F. H. C. Crick, and V. Vand. 1952. The structure of synthetic polypeptides. I. The transform of atoms on a helix. *Acta Crystal.* 5:581–586.
4. DeRosier, D. J., and A. King. 1972. Structure of the tubular variants of the head of bacteriophage T_4 (polyheads). I. Arrangement of subunits in some classes of polyheads. *J. Mol. Biol.* 65:469–488.
5. deVillafranca, G. W., and C. Marschhaus. 1963. Contraction of the A-band. *J. Ultrastruct. Res.* 9:156–165.
6. Dewey, M. M., J. K. Blasie, R. J. C. Levine, and D. E. Colflesh. 1972. Changes in A-band structure during shortening of a paramyosin-containing striated muscle. *Biophys. J.* 12: 82a.
7. Dewey, M. M., D. Colflesh, H. Terry, B. Walcott, and R. J. C. Levine. 1977. Changes in thick filament length in *Limulus* striated muscle. *J. Cell Biol.* 75:366–380.
8. Dewey, M. M., R. J. C. Levine, and D. E. Colflesh. 1973. Structure of *Limulus* striated muscle. The contractile apparatus at various sarcomere lengths. *J. Cell Biol.* 58:574–593.
9. Elliott, G. F. 1964. Electron microscope studies of the structure of the filaments in the opaque adductor muscle of the oyster *Crassostrea angulata. J. Mol. Biol.* 10:89–104.
10. Hardwicke, P. M. D., and J. Hanson. 1971. Separation of thick and thin myofilaments. *J. Mol. Biol.* 59:509–516.
11. Haselgrove, J. C. 1975. X-ray evidence for conformational changes in the myosin filaments of vertebrate striated muscle. *J. Mol. Biol.* 92:113–143.
12. Haselgrove, J. C. 1980. A model of myosin cross-bridge structure consistent with the low-angle X-ray diffraction pattern of vertebrate muscle. *J. Muscle Res. Cell Motil.* 1:177–191.
13. Horne, R. W., and R. Markham. 1972. Applications of optical diffraction and image reconstruction techniques to electron micrographs. *In* Practical Methods of Electron Microscopy. A. M. Glavert, editor. North Holland/American Elsevier. New York. 327–444.
14. Huxley, A. F., and R. Niedergerke. 1954. Structural changes in muscle during contraction. Interference microscopy of living muscle fibers. *Nature (Lond.).* 173:971–943.
15. Huxley, H. E., and W. Brown. 1967. The low-angle X-ray diagram of vertebrate striated muscle and its behavior during contraction and rigor. *J. Mol. Biol.* 30:383–434.
16. Huxley, H. E., and J. Hanson. 1954. Changes in the cross-striations of muscle during contraction and stretch and their structural interpretation. *Nature (Lond.).* 173:973–976.
17. Klug, A., and J. E. Berger. 1964. An optical method for the analysis of periodicities in electron micrographs, and some observations on the mechanism of negative staining. *J. Mol. Biol.* 10:565–569.
18. Levine, R. J. C., M. M. Dewey, and G. W. deVillafranca. 1972. Immunohistochemical localization of contractile proteins in *Limulus* striated muscle. *J. Cell Biol.* 551:221–235.
19. Miller, A., and R. T. Tregear. 1972. Structure of insect fibrillar flight muscle in the presence and absence of ATP. *J. Mol. Biol.* 70:85–104.

20. Miller, B. M., and G. Elliott. 1972. An X-ray diffraction study of contracting molluscan smooth muscle. *Biophys. J.* 12:1405–1414.
21. Morimoto, K., and W. F. Harrington. 1974. Substructure of thick filaments of vertebrate striated muscle. *J. Mol. Biol.* 83:83–97.
22. Pepe, F. A. 1971. Structure of the myosin filament in striated muscle. *Prog. Biophys. Mol. Biol.* 22:77–96.
23. Pepe, F. A. 1973. The myosin filament: immunochemical and ultrastructural approaches to molecular organization. *Cold Spring Harbor Symp. Quant. Biol.* 37:97–108.
24. Pepe, F. A., and B. Drucker. 1979. The myosin filament. VI. Myosin content. *J. Mol. Biol.* 130:379–393.
25. Reedy, M. K., G. F. Bahr, and D. A. Fischman. 1973. How many myosins per cross-bridge? I. Flight muscle from the blowfly, *Sarcophaga bullata*. *Cold Spring Harbor Symp. Quant. Biol.* 37:397–421.
26. Reedy, M. K., K. R. Leonard, R. Freeman, and T. Arad. 1981. Thick myofilament mass determination by electron scattering measurements with the scanning transmission electron microscope. *J. Mus. Res. Cell Motil.* 2:45–64.
27. Rome, E. 1972. Relaxation of glycerinated muscle: low-angle X-ray diffraction studies. *J. Mol. Biol.* 65:331–345.
28. Squire, J. M. 1971. General model for the structure of all myosin-containing filaments. *Nature (Lond.).* 223:457–462.
29. Squire, J. M. 1973. General model of myosin filament structure. III. Molecular packing arrangements in myosin filaments. *J. Mol. Biol.* 77:291–323.
30. Squire, J. M. 1975. Muscle filament structure and muscle contraction. *Annu. Rev. Biophys. Bioeng.* 4:137–163.
31. Tregear, R. T., and J. M. Squire. 1973. Myosin content and filament structure in smooth and striated muscle. *J. Mol. Biol.* 77:279–290.
32. Wray, J. S. 1979. Structure of the backbone in myosin filaments of muscle. *Nature (Lond.).* 277:37–40.
33. Wray, J. S. 1979. X-ray diffraction studies of myosin filament structures in crustacean muscles. *In* Motility in Cell Function. Proceedings of the First John M. Marshall Symposium in Cell Biology. F. A. Pepe, J. W. Sanger, and V. T. Nachmias, Academic Press, Inc., New York. 347–350.
34. Wray, J. S. 1979. Filament geometry and the activation of insect flight muscles. *Nature (Lond.).* 280:325–326.
35. Wray, J. S., P. J. Vibert, and C. Cohen. 1974. Cross-bridge arrangements in *Limulus* muscle. *J. Mol. Biol.* 88:343–348.
36. Wray, J. S., P. J. Vibert, and C. Cohen. 1975. Diversity of cross-bridge configurations in invertebrate muscles. *Nature (Lond.).* 257:561–564.
37. Wrigley, N. G. 1968. The lattice spacing of crystallic catalase as an internal standard of length in electron microscopy. *J. Ultrastruct. Res.* 24:454–464.